ADVANCED MATERIALS
www.advmat.de

Realizing Colorful Holographic Mimicry by Metasurfaces

Bo Xiong, Yihao Xu, Jianan Wang, Lin Li, Lin Deng, Feng Cheng, Ru-Wen Peng, Mu Wang,* and Yongmin Liu**

Mimicry is a biological camouflage phenomenon whereby an organism can change its shape and color to resemble another object. Herein, the idea of biological mimicry and rich degrees of freedom in metasurface designs are combined to realize holographic mimicry devices. A general mathematical method, called phase matrix transformation, to accomplish the holographic mimicry process is proposed. Based on this method, a dynamic metasurface hologram is designed, which shows an image of a "bird" in the air, and a distinct image of a "fish" when the environment is changed to oil. Furthermore, to make the mimicry behavior more generic, holographic mimicry operating at dual wavelengths is also designed and experimentally demonstrated. Moreover, the fully independent phase modulation realized by phase matrix transformation makes the working efficiency of the device relatively higher than the conventional multiwavelength holographic devices with off-axis illumination or interleaved subarrays. The work potentially opens a new research paradigm interfacing bionics with nanophotonics, which may produce novel applications for optical information encryption, virtual/augmented reality (VR/AR), and military camouflage systems.

Camouflage is the phenomenon that an animal can adapt to the surrounding environments to protect the animal from the visual detection of predators.[1–3] According to Darwin's theory of natural selection, this property can provide the animals with a reproductive advantage, enabling them to produce more offspring than the others.[4] In nature, camouflage can be achieved by various methods,[5] such as crypsis[6] and some forms of mimicry.[7] Crypsis means that with the coloration or illumination, the animals can be hardly seen and hence hidden in the environment. The examples of crypsis include the color change in chameleons[8,9] and cephalopods.[10] Mimicry is more complicated and difficult, which requires the animal to mimic another object, usually even another species, to protect itself from predators.[7] Recently, researchers have found that the complex crypsis behavior in chameleons originates from the active mechanical tuning of the lattice of guanine nanocrystals that act as photonic crystals.[8] The guanine nanocrystals can reflect light with distinct wavelengths after the tuning, giving rise to crypsis in different circumstances. Utilizing this principle, people have designed mechanical-tuning-based biomimetic elastomers to imitate the active crypsis behavioues.[9,10] The idea of crypsis has also been applied to plasmonic devices for thermal camouflage.[11–13] By tailoring the infrared emission of the nanostructures, the thermal radiation can be controlled and the temperature of the surface can maintain the same as the surrounding environment. However, the research on the other kind of camouflage, mimicry, is still challenging.

Metasurfaces,[14–19] an emerging 2D photonic platform made of subwavelength arrays of artificially designed scatters, have demonstrated many unique features that are unavailable in conventional materials.[17,20,21] Because of the exceptional ability to modify the phase,[14–16,22,23] polarization,[24–26] and amplitude[27–32] of reradiated light, metasurfaces have enabled a number of applications, including broadband wave-plates,[33,34] polarization rotators,[25,26] perfect absorbers,[27,35] metalenses,[36–39] plasmonic color display,[28,40–42] holograms,[43–47] and so on. Among them, as one important direction, tunable and reconfigurable meta-devices have attracted much attention. People have demonstrated this unique property with microelectromechanical systems,[48] mechanical deformation,[49–52] electrical stimuli,[53,54] field-programmable gate array,[55,56] and phase-transition materials,[57,58] to name a few. However, most of them require a large volume, complicated systems, or special materials. More convenient reconfigurable metasurfaces still remain great challenges. In this work, utilizing the multiple degrees of freedom in metasurface designs,[18,19] we propose and experimentally demonstrate a holographic mimicry device for the first time, which can show different images in different surrounding circumstances. To realize such a novel function, we propose a general mathematical method, called phase matrix transformation, for achieving the fully independent phase modulation and designing the objective holographic images that we want to mimic. When the metasurface works

B. Xiong, J. Wang, Prof. R.-W. Peng, Prof. M. Wang
National Laboratory of Solid State Microstructures, School of Physics, and Collaborative Innovation Center of Advanced Microstructures
Nanjing University
Nanjing 210093, China
E-mail: rwpeng@nju.edu.cn; muwang@nju.edu.cn

Y. Xu, Dr. L. Li, Prof. Y. Liu
Department of Mechanical and Industrial Engineering
Northeastern University
Boston, MA 02115, USA
E-mail: y.liu@northeastern.edu

L. Deng, Dr. F. Cheng, Prof. Y. Liu
Department of Electrical and Computer Engineering
Northeastern University
Boston, MA 02115, USA

The ORCID identification number(s) for the author(s) of this article can be found under https://doi.org/10.1002/adma.202005864.

DOI: 10.1002/adma.202005864

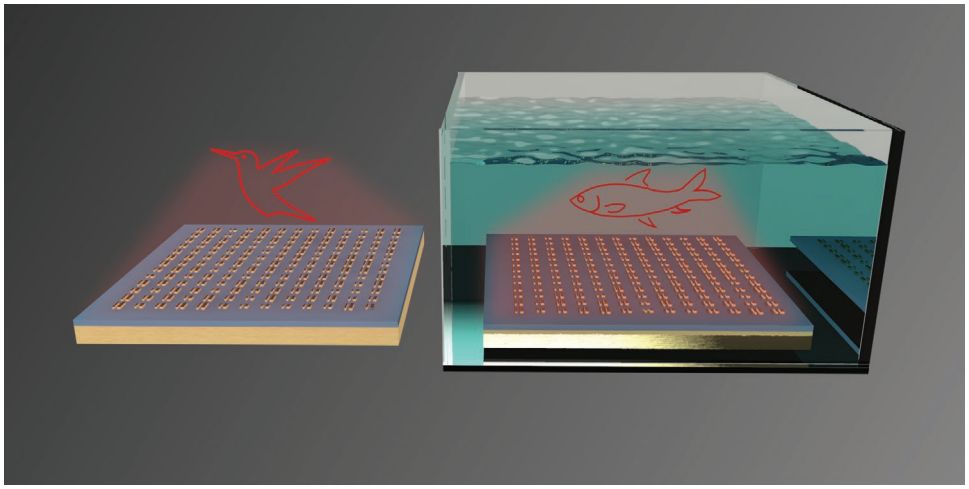

Figure 1. Schematic of the holographic mimicry by metasurfaces. For the same metasurface, when it works in one medium (e.g., air), for instance, the holographic image of a bird is perceived. In contrast, when we switch to another medium (e.g., oil or water), the holographic image is changed to a fish. The two holographic images are completely independent, which can be used for holographic mimicry.

in the air, the holographic image of a "bird" is perceived. After we immerse the metasurface into the liquid (oil in the current work), the holographic image will change to a "fish." This effect just resembles the mimicry behavior in nature. Furthermore, combined with the idea of controllable multiwavelength metasurfaces,[59–62] we design a dual-wavelength holographic mimicry device, which can show four distinct holographic images, making the mimicry behaviors more generic. Due to the fully independent phase modulation at dual wavelengths and in dual circumstances, the side images caused by the cross-talk can be largely avoided and the effective working efficiency is relatively higher than the conventional off-axis illumination design[63,64] and interleaved subarrays design.[60,65] The colorful holographic mimicry device realized by metasurfaces is a good example of interdisciplinary research by merging bionics and nanophotonics, which will inspire further development and more potential applications in both domains.

Figure 1 shows the schematics of the holographic mimicry working in different surrounding environments. For the mimicry in nature, one typical example is the genus Thaumoctopu (i.e., mimic octopus) which is able to intentionally alter their body shape to resemble dangerous sea snakes or lionfish according to different circumstances. Here, for our designed holographic mimicry metasurface, the hologram of the device would exhibit an image of a "bird" in the air. However, when the environment becomes liquid (oil in the current work), the "bird" will automatically change to a "fish" that is ubiquitous in water, accomplishing the holographic mimicry behaviors. We want to emphasize that before and after the imitation process, all the geometric parameters of the nanostructures and their arrangements on the metasurface remain the same, while the exhibited holographic images are completely independent.

The design principle of the holographic mimicry device is illustrated in **Figure 2**a. To achieve different phase responses and the desired holographic mimicry performance, we propose a general method, called phase matrix transformation. First, to generate the hologram of a bird in the air, we need to construct a specific phase profile based on the iterative Fourier transform algorithm.[47] Here, we adopt 4-level phases,[44] which are labeled by 1, 2, 3, and 4 in the inset of Figure 2a, and thus the specific phase profile can be rewritten as a phase matrix P1 as shown in Figure 2a. Each matrix element stands for one pixel on the metasurfaces. Second, another specific matrix P2 can be determined in a similar manner to realize the holographic image of a fish in the oil. Once we construct a specific nanostructure whose optical response can be independently controlled in two different environments due to the change of index, the phase of the nanostructure in the air and oil could be arbitrary values according to our design. With such a specific nanostructure to build the metasurface, the phase mapping in the air and oil can be designed as matrix P1 and P2, respectively. In this case, when we change the surrounding environment from air to oil, the phase matrix transformation from P1 to P2 can be implemented, and thus holographic mimicry effect can be realized.

To accomplish the phase matrix transformation method, the designed unit element should be elaborately designed and optimized. First, the structure needs to support multiple resonant modes, which can provide independent optical responses in different environments. Second, these resonant modes need to be quite sensitive to the surrounding medium, in order to realize a phase shift approaching 2π when the refractive index of the surround medium changes. Here, we design a coupled metal–insulator–metal structure as the unit cell, which is shown in Figure 2b. It is composed of a 100 nm thick gold substrate, 50 nm thick SiO_2 spacing layer, and gold nanoantennas on the top with 40 nm thickness. The period is 500 and 250 nm along the x- and y-direction, respectively. In each period, there are two coupled nanobars with different geometric parameters, which can support multiple resonant modes as indicated in Figure 2c,d. We have also used finite-difference time-domain (FDTD) simulations to calculate the reflectance and field distribution of the unit cells. The refractive index of oil used in the simulation is $n = 1.515$, and the complex permittivity of gold in the working wavelength regime is described by the Drude model that matches the experimentally obtained value.[66] The geometric parameters of these two nanobars in the figure are

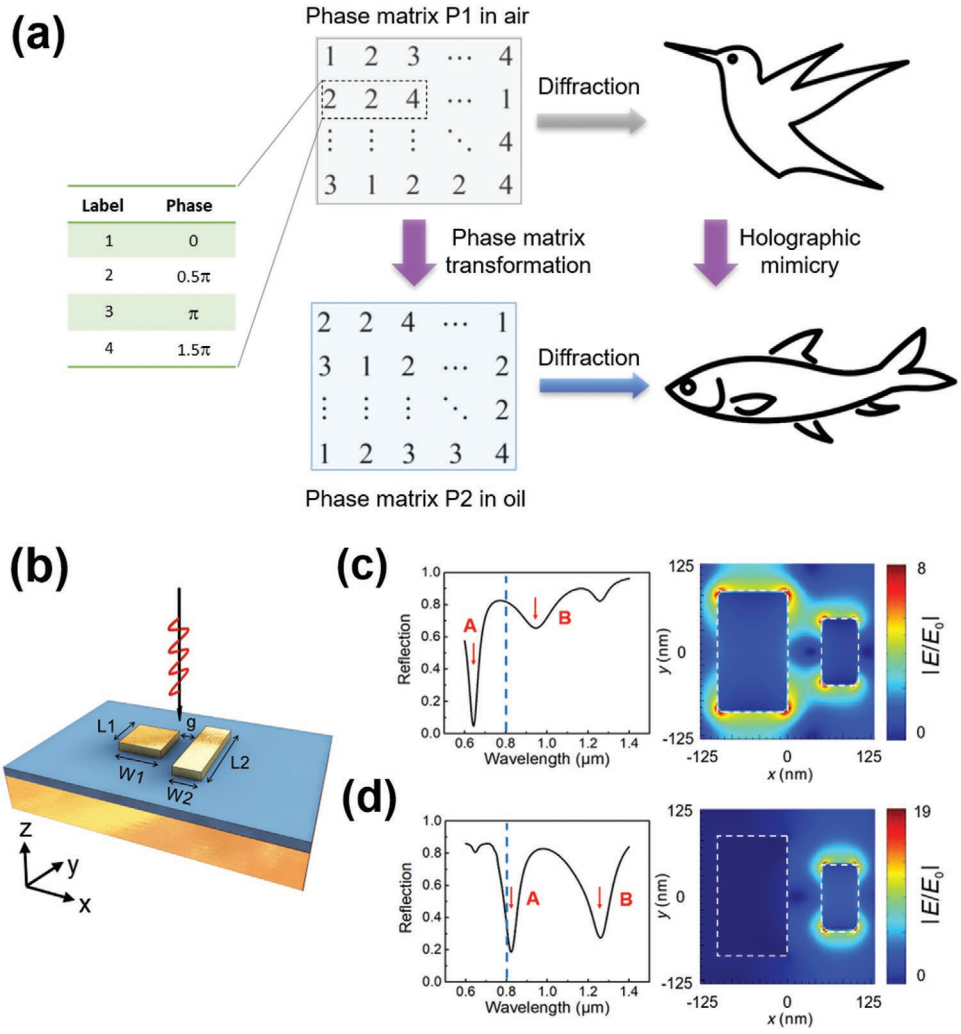

Figure 2. Phase matrix transformation method and design of the unit cell. a) The phase matrix transformation method to realize holographic mimicry via a four-level phase discretization. The phase matrix in the air is P1, which can show a hologram pattern of a bird. If the phase matrix P1 transfers to another one P2, the hologram pattern can change to a fish. b) Schematic of the composite unit cell consisting of two gold nanobars. c,d) In the air (c) and oil (d), the calculated reflected spectrum of a composite unit cell with geometry $L_1 = 172$nm, $L_2 = 97$ nm, $W_1 = 100$ nm, $W_2 = 50$ nm, and $g = 40$ nm. The individual resonances A and B, marked by the red arrows, would shift to the longer wavelengths when the surrounding medium is changed from air to oil. The working wavelength is 800 nm as indicated by the blue dashed line.

$L_1 = 172$, $L_2 = 97$, $W_1 = 100$, $W_2 = 50$, and $g = 50$ nm. The incident light is linearly polarized along the *y*-direction. The simulated reflected spectra in the air (Figure 2c) and oil (Figure 2d) demonstrate that, after immersing the sample into oil, the two resonant modes, marked by the red arrows, would shift to the longer wavelength because of the increased refractive index of the surrounding medium. From the simulated electric field intensity at the working wavelength 800 nm (the blue dashed line), we can see that the mode in the air is a coupled mode between the two bars, while in the oil it is an electric dipole of the single right bar, resulting in two different phase responses equal to zero (in the air) and π (in the oil), respectively. These results demonstrate that the excited localized surface plasmon modes are quite sensitive to the surrounding environment, which satisfy the requirement as mentioned above. Then we swept L1 and L2 from 40 to 220 nm while fixing the other geometric parameters to search the rest necessary phase response. The searched results are listed in Figure S1 and Table S1 in the Supporting Information. With the 16 different unit cells, the designed metasurface can generate an arbitrary phase matrix (e.g., P1) in the air and another arbitrary phase matrix (e.g., P2) in the oil, because we only need 16 mapping relationships during the transferring process of phase matrix.

The holographic mimicry metasurface, composed of 400 × 800 pixels with an overall dimension of 200 × 200 μm, was fabricated by standard e-beam lithography. The optical and scanning electron microscopy (SEM) images of the fabricated sample are shown in **Figure 3**a,b, respectively. It is clear that in different pixels, the geometrics of the gold nanorods are different. We used a customized optical setup to characterize the device (see Figure S2 in the Supporting Information). To demonstrate the holographic mimicry, we covered the metasurface with cedar oil ($n = 1.515$) and sealed it in a cell. The simulated and measured holographic mimicry results are shown in

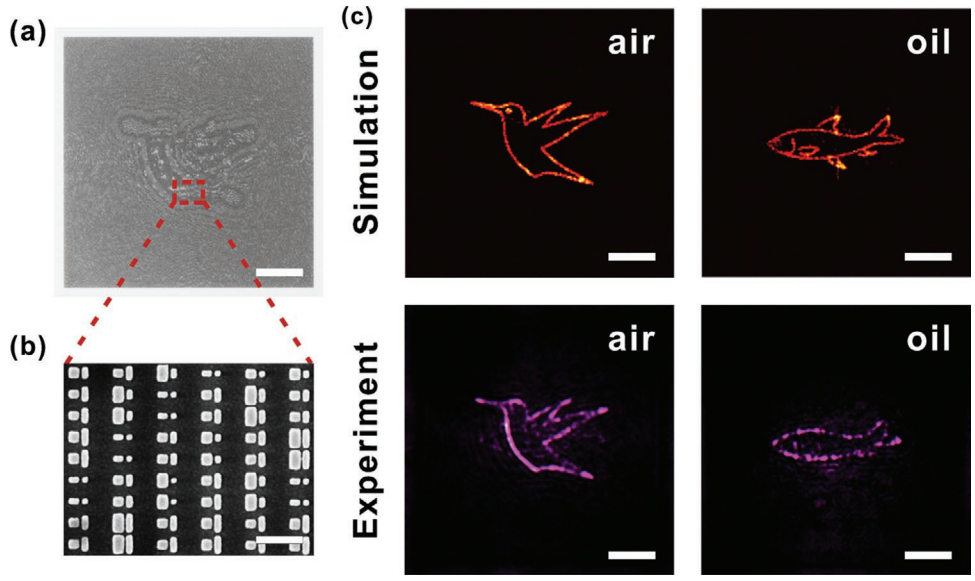

Figure 3. Experimental results of single-wavelength holographic mimicry. a) Optical and b) SEM images of the holographic mimicry sample. The scale bars are 40 μm in (a) and 500 nm in (b). c) Simulated holographic images and measured results in the air (left) and oil (right) at the wavelength of 800 nm. All the scale bars in (c) are 40 μm.

Figure 3c. We can clearly observe that the holographic image transitions from a "bird" to a "fish" when the surrounding environment changes from air to oil. This effect is very similar to the mimicry behavior of octopus, confirming that we have realized the holographic mimicry with the "phase matrix transformation" design in metasurfaces. It should be pointed out that there are still some distortions and speckles in the observed holograms, which originate from the four-level phase in our design and the imperfection in sample fabrication. The performance could be further improved by optimizing the structural configuration to realize higher-level phase modulation. In addition, the working efficiency is an important metric of the hologram device, which is defined as ratio of the integrated intensity of the hologram patterns to the light incident on the sample. The integrated intensity is obtained by integrating the light intensity pixel by pixel in the image plane with the same size and same position of the designed pattern. In our work, the efficiencies for the device in the air and oil at the working wavelength (800 nm) are about 17.61% and 15.46%, respectively (see Figure S3 in the Supporting Information). The energy losses are mainly due to the scattering and the absorption of the coupled nanobars. Moreover, to demonstrate the dependence of the device's performance on the incident wavelength and surrounding refractive index, we have also simulated a focusing sample by FDTD as presented in Figures S4 and S5 in the Supporting Information. Through sweeping the incident wavelength and refractive index, the simulated results indicate that when the index value deviates from air and oil or the wavelength deviates from 800 nm, the intensity of the focal point will decrease. This is because the excited resonant modes in nanostructures are rather sensitive to these parameters.

In the following, we show that holographic mimicry can be extended to multiple wavelengths. Wavelength is a critical degree of freedom for multifunction metasurfaces.[59–62] With proper designs, metasurfaces could manipulate light in an independent manner and realize independent functions at different working wavelengths. This idea can also be introduced to the holographic mimicry device. In nature, animals are usually colorful. If the metasurface hologram can operate at more than one wavelength, which means a colorful hologram, the holographic mimicry will be more attractive. Here we have successfully demonstrated a dual-wavelength holographic mimicry device. The unit cell, as shown in **Figure 4**a, now consists of three gold nanobars, which provide more degrees of freedom in geometric parameters than the previous design. We vary the length of the three nanobars (L_1, L_2, and L_3) to search the necessary parameters, while the widths of the nanobars and their separation distance are fixed ($W_1 = 60$ nm, $W_2 = 80$ nm, $W_3 = 100$ nm, and $g = 40$ nm). The period is 500 nm in both the x- and the y-direction. The optimized working wavelengths are set as 710 and 890 nm. The simulation details and the required parameter groups are presented in the Supporting Information (see Figures S6, S7, and Table S2). Here, for simplicity we only adopt a two-level phase quantization in the design of hologram. However, four-level or even higher-level quantization can also be realized by introducing more degrees of freedom in geometric parameters. For example, we can further change the orientation angles of the coupled nanobars in different pixels to combine the geometric phase and propagation phase. Consequently, multiple functions can be integrated within a single metadevice.[67,68]

As the proof-of-principle demonstration of the wavelength-controlled function in different circumstances, we have designed a simple focusing experiment, in which for two wavelengths and two surrounding media (air and oil), there are four independent focal points at different spatial positions. The results are presented in Figure S8 in the Supporting Information, indicating that dual-wavelength dynamic holographic images are possible by a single metasurface. Figure 4a,b illustrates the design and concept of colorful holographic mimicry.

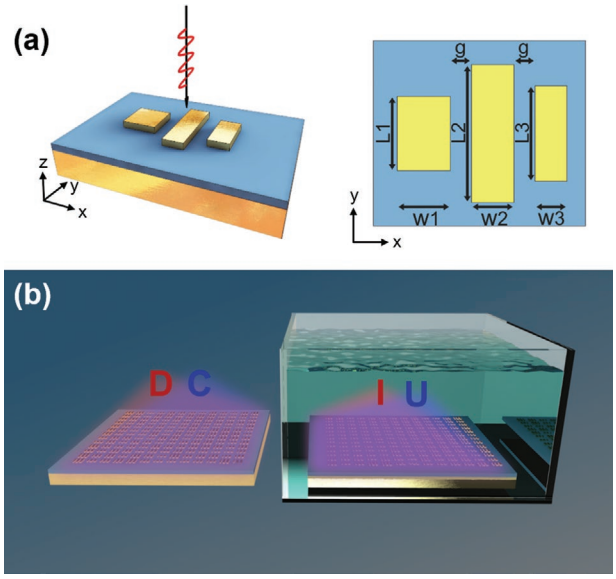

Figure 4. Design principle and schematics for colorful holographic mimicry. a) Schematic of the composite unit cell, which contains three bars in one period. The incident light is polarized along the *y*-direction. Here we fix $g = 40$ nm, $W_1 = 60$ nm, $W_2 = 80$ nm, and $W_3 = 100$ nm. Then we vary L_1, L_2 and L_3 to search the necessary parameters. The period is 500 nm in both directions. b) For different surrounding media and different wavelengths, four independent holographic patterns can be generated. Here, letters of "D"/"I" and "C"/"U" are the corresponding holographic images working at 710 nm and 890 nm, respectively. In this configuration, colorful holographic mimicry can be realized.

When the environment is air, the holographic image is a letter of "D" at 710 nm wavelength, and changes to a letter of "C" at 890 nm. This means a colorful holographic image of "DC" can be realized when working in the air. After the whole sample is covered by cedar oil, the holographic image of "D" changes to "I" and "C" turns to "U". Therefore, a completely different colorful holographic image, "IU", would emerge, realizing the colorful holographic mimicry. The experimental results are shown in **Figure 5**. The size of the metasurface sample is 200 × 200 μm, which contains 400 × 400 pixels. The imaging plane of the hologram is set at 500 μm above the metasurface. Figure 5a shows the optical image of the entire metasurface, while the SEM image of the sample is presented in Figure 5b. The smallest nanoantenna only has a width of 60 nm and a length of 40 nm. The simulated and measured holographic images are shown in Figure 5c. We can clearly see that the positions and patterns of the images in the experiment are very close to the design, verifying the good performance of colorful holographic mimicry. Although there are some distortions in the holographic images, which likely originate from the imperfect fabrication process, they can be further improved by optimizing the design and fabrication. The working efficiencies for the dual-wavelength holographic mimicry device are about 11.47% (710 nm in the air), 13.48% (890 nm in the air), 12.84% (710 nm in the oil), and 11.61% (890 nm in the oil). Due to the strict requirement of independent phase control at dual wavelengths and in dual circumstances, we sacrifice the optimization for the reflective amplitude, and hence the efficiencies are a little lower than the single-wavelength holographic mimicry device. However, it is still relatively higher than traditional metasurface systems which utilize off-axis illumination method[63,64] or interleaved subarrays method[60,65] to realize the multiwavelength hologram. This is because with these traditional methods, the phase for different wavelengths are not independent and several unwanted side images are generated at the same time, leading to significant decrease in the efficiency. Meanwhile, in our work, independent phase modulation can be fully realized by phase matrix transformation, which eliminates side images and results in the relatively high efficiency of the sample. Such advantages make our holographic mimicry device suitable for real applications.

In this experiment, we only consider the holographic images working at two discrete wavelengths, which are modified by two resonant modes of the nanostructures as discussed in Figure S6 (Supporting Information). From the simulated reflection spectra in Figure S6 (Supporting Information), we can see that there are five dips in total from 600 to 1200 nm. This indicates that five different resonant modes can be excited. In this case, we can further realize five holographic images at the corresponding wavelengths, making the colorful holograms more vivid and attractive. However, to modify these wavelengths, besides the length of the three nanobars, we may need to sweep more geometric parameters to find the required phase response, such as the width of each bar and the separation gaps. Moreover, the holography mimicry can also be easily switched back and forth by integrating the device with a microfluid cell,[69] where the sample is sealed in a cell and the liquid can flow in/out through the solution inlet/outlet with a syringe. In this case, the oil with high adhesion used in our work should be replaced with other liquid with a similar refractive index and low adhesion. We will explore these advanced designs in the future.

To summarize, we have combined the idea of biological mimicry and metasurface hologram and realized holographic mimicry for the first time. Like the natural animals' mimicry behavior, the holographic image can automatically turn into another independent pattern when the environment is changed. To achieve such a novel function, we design a unit cell consisting of coupled gold naonbars and propose a general design method, "phase matrix transformation," to construct the metasurface device. Through sweeping the geometric parameters of the nanobars, we have found all the required unit cells to accomplish the mimicry process. The experimental results demonstrate that a "bird" in the air can be changed to a "fish" after submerging the device in the oil. Furthermore, we introduce wavelength as an extra degree of freedom to design a colorful holographic mimicry device, making the mimicking behaviors more generic. When the environment changes, a colorful holographic image of "D" at 710 nm and "C" at 890 nm will automatically turn into "I" and "U", respectively. To the best of our knowledge, this is the first experimental demonstration of a dynamic multiwavelength holographic device. The effective working efficiency is reasonably high due to the fully independent control at dual wavelengths and in dual circumstances, in comparison with the traditional multiwavelength holographic devices. Very recently, machine learning and deep learning have been applied to design distinct photonic structures, which can help to unlock the highly nonlinear structure–property relationship.[70,71] Using such a data-driven

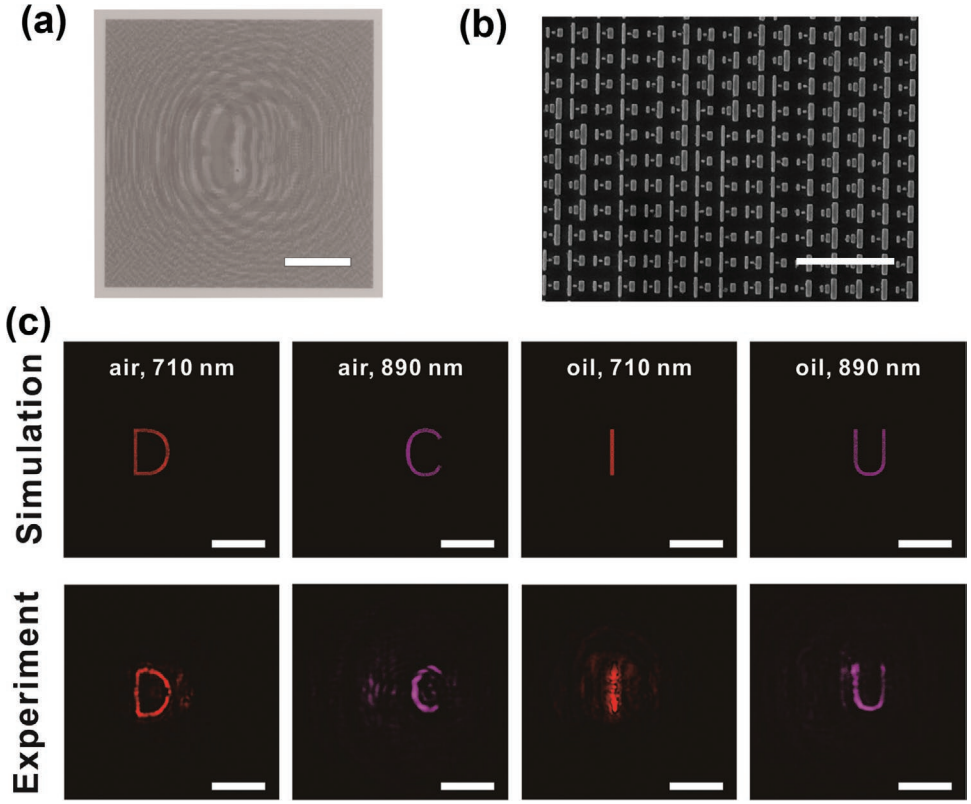

Figure 5. Experimental results of dual-wavelength holographic mimicry. a) Optical and b) SEM images of the colorful holographic mimicry sample. The scale bar is 50 μm in (a) and 2 μm in (b). c) Simulated (top) and experimental (bottom) results of the colorful holographic mimicry. With 710 nm light incident in air, the holographic picture shows a letter of "D", while it changes to a letter of "C" at the wavelength of 890 nm. For the same metasurface, if we cover the whole sample with cedar oil, the hologram pictures at 710 nm and 890nm are "I" and "U", respectively. All the scale bars in (c) are 50 μm.

inverse design framework, we can search the proper geometrical parameters of unit elements more quickly and accurately. As a result, more resonant modes of complex structures can be utilized to realize multifunctional capabilities. In addition, we can make the holographic mimicry sensitive to other degrees of freedom, including polarization,[45] orbital angular momentum[72] as well as perceiving angles.[73] We believe that our work opens a new way for interdisciplinary research that interfaces bionics and nanophotonics. It will find many applications for optical information encryption, multifunction optical devices, AR/VR, and military camouflage.

Supporting Information

Supporting Information is available from the Wiley Online Library or from the author.

Acknowledgements

Y.L. acknowledges the financial support from the National Science Foundation (Nos. ECCS-1916839 and CBET-1931777). R.-W.P., M.W., B.X., and J.W. acknowledge the financial support from the National Key R&D Program of China (Grant Nos. 2020YFA0211300 and 2017YFA0303702), and the National Natural Science Foundation of China (Grants Nos. 11634005, 61975078, 11674155, and 11974177).

Conflict of Interest

The authors declare no conflict of interest.

Data Availability Statement

The data that support the findings of this study are available from the corresponding author upon reasonable request.

Keywords

adaptive camouflage, biological mimicry, dynamic metasurfaces, multiwavelength holograms

Received: August 28, 2020
Published online:

[1] E. B. Poulton, *The Colours of Animals: Their Meaning And Use: Especially Considered in The Case of Insects*, Trübner & Company, New York **1890**.
[2] K. W. McKee, D. W. Tack, *Active Camouflage for Infantry Headwear Applications*, HumanSystems Inc, Guelph, ON, Canada **2007**.
[3] P. Forbes, *Dazzled and Deceived: Mimicry and Camouflage*, Yale University Press, New Haven, CT, USA **2011**.

[4] C. Darwin, *Mentor Edition*, New American Library, New York, **1859**.
[5] M. Stevens, S. Merilaita, *Phil. Trans. R. Soc. B* **2009**, *364*, 423.
[6] M. Allaby, *A Dictionary of Zoology*, Oxford University Press, Oxford, UK, **2003**.
[7] R. I. Vane-Wright, *Biol. J. Linn. Soc.* **1980**, *13*, 1.
[8] J. Teyssier, S. V. Saenko, D. Van Der Marel, M. C. Milinkovitch, *Nat. Commun.* **2015**, *6*, 6368.
[9] M. Vatankhah-Varnosfaderani, A. N. Keith, Y. Cong, H. Liang, M. Rosenthal, M. Sztucki, C. Clair, S. Magonov, D. A. Ivanov, A. V. Dobrynin, *Science* **2018**, *359*, 1509.
[10] C. Xu, G. T. Stiubianu, A. A. Gorodetsky, *Science* **2018**, *359*, 1495.
[11] L. Xiao, H. Ma, J. Liu, W. Zhao, Y. Jia, Q. Zhao, K. Liu, Y. Wu, Y. Wei, S. Fan, *Nano Lett.* **2015**, *15*, 8365.
[12] Y. Qu, Q. Li, L. Cai, M. Pan, P. Ghosh, K. Du, M. Qiu, *Light: Sci. Appl.* **2018**, *7*, 26.
[13] O. Salihoglu, H. B. Uzlu, O. Yakar, S. Aas, O. Balci, N. Kakenov, S. Balci, S. Olcum, S. Süzer, C. Kocabas, *Nano Lett.* **2018**, *18*, 4541.
[14] N. Yu, P. Genevet, M. A. Kats, F. Aieta, J.-P. Tetienne, F. Capasso, Z. Gaburro, *Science* **2011**, *334*, 333.
[15] X. Ni, N. K. Emani, A. V. Kildishev, A. Boltasseva, V. M. Shalaev, *Science* **2012**, *335*, 427.
[16] S. Sun, Q. He, S. Xiao, Q. Xu, X. Li, L. Zhou, *Nat. Mater.* **2012**, *11*, 426.
[17] N. Yu, F. Capasso, *Nat. Mater.* **2014**, *13*, 139.
[18] S. Chen, Z. Li, W. Liu, H. Cheng, J. Tian, *Adv. Mater.* **2019**, *31*, 1970118.
[19] B. Xiong, L. Deng, R. Peng, Y. Liu, *Nanoscale Adv.* **2019**, *1*, 3786.
[20] Y. Liu, X. Zhang, *Chem. Soc. Rev.* **2011**, *40*, 2494.
[21] R. Fan, B. Xiong, R. Peng, M. Wang, *Adv. Mater.* **2020**, *32*, 1904646.
[22] A. V. Kildishev, A. Boltasseva, V. M. Shalaev, *Science* **2013**, *339*, 1232009.
[23] S. Chen, Z. Li, Y. Zhang, H. Cheng, J. Tian, *Adv. Opt. Mater.* **2018**, *6*, 1800104.
[24] Y.-J. Gao, X. Xiong, Z. H. Wang, F. Chen, R.-W. Peng, M. Wang, *Phys. Rev. X* **2020**, *10*, 031035.
[25] R.-H. Fan, Y. Zhou, X.-P. Ren, R.-W. Peng, S.-C. Jiang, D.-H. Xu, X. Xiong, X.-R. Huang, M. Wang, *Adv. Mater.* **2015**, *27*, 1201.
[26] N. K. Grady, J. E. Heyes, D. R. Chowdhury, Y. Zeng, M. T. Reiten, A. K. Azad, A. J. Taylor, D. A. Dalvit, H.-T. Chen, *Science* **2013**, *340*, 1304.
[27] X. Xiong, S.-C. Jiang, Y.-H. Hu, R.-W. Peng, M. Wang, *Adv. Mater.* **2013**, *25*, 3994.
[28] F. Z. Shu, F. F. Yu, R. W. Peng, Y. Y. Zhu, B. Xiong, R. H. Fan, Z. H. Wang, Y. Liu, M. Wang, *Adv. Opt. Mater.* **2018**, *6*, 1700939.
[29] J. Lin, P. Genevet, M. A. Kats, N. Antoniou, F. Capasso, *Nano Lett.* **2013**, *13*, 4269.
[30] L. Liu, X. Zhang, M. Kenney, X. Su, N. Xu, C. Ouyang, Y. Shi, J. Han, W. Zhang, S. Zhang, *Adv. Mater.* **2014**, *26*, 5031.
[31] M. Decker, I. Staude, M. Falkner, J. Dominguez, D. N. Neshev, I. Brener, T. Pertsch, Y. S. Kivshar, *Adv. Opt. Mater.* **2015**, *3*, 813.
[32] Z. Su, F. Cheng, L. Li, Y. Liu, *ACS Photonics* **2019**, *6*, 1947.
[33] N. Yu, F. Aieta, P. Genevet, M. A. Kats, Z. Gaburro, F. Capasso, *Nano Lett.* **2012**, *12*, 6328.
[34] S.-C. Jiang, X. Xiong, Y.-S. Hu, Y.-H. Hu, G.-B. Ma, R.-W. Peng, C. Sun, M. Wang, *Phys. Rev. X* **2014**, *4*, 021026.
[35] N. Liu, M. Mesch, T. Weiss, M. Hentschel, H. Giessen, *Nano Lett.* **2010**, *10*, 2342.
[36] M. Khorasaninejad, W. T. Chen, R. C. Devlin, J. Oh, A. Y. Zhu, F. Capasso, *Science* **2016**, *352*, 1190.
[37] S. Wang, P. C. Wu, V.-C. Su, Y.-C. Lai, M.-K. Chen, H. Y. Kuo, B. H. Chen, Y. H. Chen, T.-T. Huang, J.-H. Wang, *Nat. Nanotechnol.* **2018**, *13*, 227.
[38] Z. Li, K. Yao, F. Xia, S. Shen, J. Tian, Y. Liu, *Sci. Rep.* **2015**, *5*, 12423.
[39] M. Khorasaninejad, F. Capasso, *Science* **2017**, *358*, eaam8100.
[40] Z.-H. Wang, Y.-S. Hu, X. Xiong, R.-W. Peng, M. Wang, *Opt. Lett.* **2017**, *42*, 1153.
[41] X. Duan, S. Kamin, N. Liu, *Nat. Commun.* **2017**, *8*, 14606.
[42] A. Kristensen, J. K. Yang, S. I. Bozhevolnyi, S. Link, P. Nordlander, N. J. Halas, N. A. Mortensen, *Nat. Rev. Mater.* **2017**, *2*, 16088.
[43] X. Ni, A. V. Kildishev, V. M. Shalaev, *Nat. Commun.* **2013**, *4*, 2807.
[44] G. Zheng, H. Mühlenbernd, M. Kenney, G. Li, T. Zentgraf, S. Zhang, *Nat. Nanotechnol.* **2015**, *10*, 308.
[45] J. B. Mueller, N. A. Rubin, R. C. Devlin, B. Groever, F. Capasso, *Phys. Rev. Lett.* **2017**, *118*, 113901.
[46] L. Jin, Z. G. Dong, S. T. Mei, Y. F. Yu, Z. Wei, Z. Y. Pan, S. D. Rezaei, X. Li, A. I. Kuznetsov, Y. S. Kivshar, J. K. Yang, C. W. Qiu, *Nano Lett.* **2018**, *18*, 8016.
[47] Z. Shi, M. Khorasaninejad, Y.-W. Huang, C. Roques-Carmes, A. Y. Zhu, W. T. Chen, V. Sanjeev, Z.-W. Ding, M. Tamagnone, K. Chaudhary, R. C. Devlin, C. W. Qiu, F. Capasso, *Nano Lett.* **2018**, *18*, 2420.
[48] E. Arbabi, A. Arbabi, S. M. Kamali, Y. Horie, M. F. Dana, A. Faraon, *Nat. Commun.* **2018**, *9*, 812.
[49] H. S. Ee, R. Agarwal, *Nano Lett.* **2016**, *16*, 2818.
[50] Z. J. Wang, L. Q. Jing, K. Yao, Y. H. Yang, B. Zheng, C. M. Soukoulis, H. S. Chen, Y. M. Liu, *Adv. Mater.* **2017**, *29*, 1700412.
[51] Z. G. Liu, H. F. Du, J. F. Li, L. Lu, Z. Y. Li, N. X. Fang, *Sci. Adv.* **2018**, *4*, eaat4436.
[52] M. Lapine, I. V. Shadrivov, D. A. Powell, Y. S. Kivshar, *Nat. Mater.* **2012**, *11*, 30.
[53] J. V. D. Groep, J. H. Song, U. Celano, Q. Li, P. G. Kik, M. L. Brongersma, *Nat. Photonics* **2020**, *14*, 426.
[54] L. Kang, Y. H. Cui, S. F. Lan, S. P. Rodrigues, M. L. Brongersma, W. S. Cai, *Nat. Commun.* **2014**, *5*, 4680.
[55] T. J. Cui, M. Q. Qi, X. Wan, J. Zhao, Q. Cheng, *Light: Sci. Appl.* **2014**, *3*, e218.
[56] L. Li, T. J. Cui, W. Ji, S. Liu, J. Ding, X. Wan, Y. B. Li, M. Jiang, C.-W. Qiu, S. Zhang, *Nat. Commun.* **2017**, *8*, 197.
[57] X. Y. Duan, N. Liu, *ACS Nano* **2018**, *12*, 8817.
[58] J. X. Li, S. Kamin, G. X. Zheng, F. Neubrech, S. Zhang, N. Liu, *Sci. Adv.* **2018**, *4*, eaar6768.
[59] W. T. Chen, K.-Y. Yang, C.-M. Wang, Y.-W. Huang, G. Sun, I.-D. Chiang, C. Y. Liao, W.-L. Hsu, H. T. Lin, S. Sun, *Nano Lett.* **2013**, *14*, 225.
[60] B. Wang, F. Dong, Q.-T. Li, D. Yang, C. Sun, J. Chen, Z. Song, L. Xu, W. Chu, Y.-F. Xiao, Q. H. Gong, Y. Li, *Nano Lett.* **2016**, *16*, 5235.
[61] Y.-W. Huang, W. T. Chen, W.-Y. Tsai, P. C. Wu, C.-M. Wang, G. Sun, D. P. Tsai, *Nano Lett.* **2015**, *15*, 3122.
[62] O. Avayu, E. Almeida, Y. Prior, T. Ellenbogen, *Nat. Commun.* **2017**, *8*, 14992.
[63] W. W. Wan, J. Gao, X. D. Yang, *ACS Nano* **2016**, *10*, 10671.
[64] X. Li, L. W. Chen, Y. Li, X. H. Zhang, M. B. Pu, Z. Y. Zhao, X. L. Ma, Y. Q. Wang, M. H. Hong, X. G. Luo, *Sci. Adv.* **2016**, *2*, e1601102.
[65] Y. W. Huang, W. T. Chen, W. Y. Tsai, P. C. Wu, C. M. Wang, G. Sun, P. Tsai D, *Nano Lett.* **2015**, *15*, 3122.
[66] P. B. Johnson, R. W. Christy, *Phys. Rev. B* **1972**, *6*, 4370.
[67] F. Zhang, M. B. Pu, J. Luo, H. L. Yu, X. G. Luo, *Opto-Electron. Eng.* **2017**, *44*, 319.
[68] F. Zhang, X. Xie, M. B. Pu, Y. H. Guo, X. L. Ma, X. Li, J. Luo, Q. He, H. L. Yu, X. G. Luo, *Adv. Mater.* **2020**, *32*, 1908194.
[69] D. Pletcher, R. A. Green, R. C. D. Brown, *Chem. Rev.* **2018**, *118*, 4573.
[70] W. Ma, F. Cheng, Y. Liu, *ACS Nano* **2018**, *12*, 6326.
[71] W. Ma, Z. Liu, Z. A. Kudyshev, A. Boltasseva, W. Cai, Y. Liu, *Nat. Photonics* **2021**, *15*, 77.
[72] J. Wang, J. Y. Yang, I. M. Fazal, N. Ahmed, Y. Yan, H. Huang, Y. X. Ren, Y. Yue, S. Dolinar, M. Tur, A. E. Willner, *Nat. Photonics* **2012**, *6*, 488.
[73] S. M. Kamali, E. Arbabi, A. Arbabi, Y. Horie, M. Faraji-Dana, A. Faraon, *Phys. Rev. X* **2017**, *7*, 041056.